IEEE Access
Multidisciplinary ⋮ Rapid Review ⋮ Open Access Journal

Received 11 February 2023, accepted 8 April 2023, date of publication 14 April 2023, date of current version 19 April 2023.

Digital Object Identifier 10.1109/ACCESS.2023.3267298

APPLIED RESEARCH

Analysis, Diagnosis and Reconfiguration of a Synchronous Motor Control With Faulty DC Link Voltage Measurement

PHILIPP HEIL AND ABID ALI

Department of Electrical Engineering, Technical University of Applied Sciences Würzburg-Schweinfurt, 97421 Schweinfurt, Germany

Corresponding author: Philipp Heil (philipp-heil@gmx.de)

This work was supported in part by the Bavarian Research Foundation.

ABSTRACT This paper discusses the effects of an incorrectly measured DC link voltage in a synchronous drive system. As the investigations show, the control algorithm can become unstable when the measured value for the DC link voltage is much smaller than the actual value. Therefore, this paper also presents two approaches for estimating the DC link voltage based on the measured currents, the motor speed and the duty cycle. If measured and estimated values of the DC link voltage deviate too much from each other, a fault diagnosis system detects this fault and enables different flags based on the fault scenario. The flags are then used to reconfigure the control algorithm, so that instead of the measured voltage its estimated value is used. The analysis shows the need for the reconfiguration of a faulty DC link voltage measurement and the experimental results demonstrate the effectiveness of the approach.

INDEX TERMS DC link voltage, fault diagnosis, observer, PMSM, reconfiguration, recursive least squares, sensor faults, voltage source inverter.

I. INTRODUCTION

In the recent past, a lot of researchers investigated several faults in electric drive systems, especially those equipped with an inverter and a permanent magnet synchronous motor (PMSM). While different faults in the inverter or the PMSM itself are often discussed [1], there is still work to do when it comes to sensor faults. With an increasing number of safety-critical applications that rely on feedback control, like electric vehicles or collaborative robots, the focus of current research is shifting to sensor faults in PMSM drives [2], [3], [4], [5], [6].

The main function of fault diagnosis is to detect and isolate faults in a system. What all diagnostic strategies have in common is that redundant information about the system is required, which has to be obtained in different ways. This redundancy can be generated either physically or analytically. To avoid additional hardware (e.g. redundant sensors), often observers are developed to estimate system quantities based on other available measurements. By comparing measured and estimated values, faults in the system can be detected and isolated [7], [8], [9].

If the fault was isolated, the control scheme can be adjusted by a reconfiguration method and faulty or failed sensor signals are replaced by calculated alternative signals. Especially in case of a complete sensor outage, the reconfiguration ensures the availability of closed loop control. Under certain circumstances, the model of the system must also be updated. By reconfiguring the system, it can remain in operation despite the presence of an error (e.g. a failed sensor). By combining fault diagnosis and a reconfiguration method, a fault-tolerant control system is created [10], [11], [12].

Permanent magnet synchronous motors are almost exclusively operated with an inverter. For its safe operation and proper control, the DC link voltage applied to the inverter must be correctly measured in addition to other variables, like speed and currents. If sensors do not function as expected, provide incorrect measured values or fail completely, problems will arise with regard to the control strategy. However, among all the sensors typically used in order to control a PMSM, the DC link voltage sensor has been the least studied one.

The associate editor coordinating the review of this manuscript and approving it for publication was Wonhee Kim.

In [13] the authors consider the PMSM drive of an electric vehicle, where two phase currents, the rotor position and the DC link voltage are being measured. A faulty DC link voltage measurement is detected by comparing the estimated electrical input power supplied to the PMSM and the mechanical output power. By using a power balance equation and assuming that the power loss within the machine and the inverter are known precisely enough, a DC link voltage sensor fault is detected, when this power balance exceeds a certain threshold. In this case the measured DC link voltage is replaced by the nominal value. This is one disadvantage of the approach, since no estimated value for the quantity to be replaced is generated. Another drawback the authors mention is the fact, that the fault detection is difficult at low speeds or in an operating point with small load, since the power itself is very small.

Diao [14], [15] introduces an observer for estimating the DC link voltage. The observer uses a single-phase current sensor, a DC link current sensor as well as the rotor speed and the gate signals of the inverter to generate the estimated value. A DC link voltage sensor fault is detected when the difference between measured and estimated value exceeds 5% of the nominal DC link voltage. The approach shows good results, but has one big disadvantage. In order to estimate the DC link voltage and detect faults concerning its measurement, another sensor (DC link current sensor) is needed, which is typically not required in order to control the motor (since the phase currents get measured already).

Another approach [16] uses an Extended Kalman Filter to estimate the currents in the stationary reference frame. Estimated and measured values for the phase currents are fed into an evaluation block. Within this block, three specially designed indices are used to locate faults in the measurement of the currents, the rotor position and the DC link voltage. Results show the effectiveness of the approach, at least for faults that occur suddenly. However, there is no possibility to reconfigure the control scheme apart from using the nominal DC link voltage, since no estimated value is calculated.

The authors in [17] propose a fault detection for the DC link voltage sensor and a fault-tolerant control scheme for a three-phase AC/DC converter. In this case a Luenberger observer is used to estimate the DC link voltage. For doing this, the converter is modeled as a nonlinear system based on the power balance equation involving input and output. At first, the nonlinearity of the model is linearized using a small signal analysis. After that, a Luenberger observer is designed to estimate the DC link voltage based on the measurements of the three phase voltages. For detecting a sensor fault, measured and estimated value of the DC link voltage are compared. In case of a fault, the measurement gets replaced by the estimation within the control loop. The results show the effectiveness of the approach. However, the application of the method is limited to the availability of phase voltage measurements.

For the reasons mentioned above and in comparison to the references cited previously, this paper presents two methods for estimating the DC link voltage, that only use the measured quantities that are needed for motor control anyway. The estimated value is used for fault diagnosis and reconfiguration. Unlike in the cited works, the DC link voltage does not only get supervised, but also an estimated value is calculated. When comparing this signal to the measured quantity, a faulty sensor can be detected and the estimated value is used to replace it. This is another contribution of this paper, since the control algorithm does not have to rely on a fixed nominal value, which is typically being used, when the DC link voltage sensor fails.

The paper is organized as follows: Section II gives a short overview of the considered system. In Section III, the impact of an incorrectly measured DC link voltage on the control algorithm is discussed. The analysis shows the need for the reconfiguration of the faulty sensor. Section IV proposes an observer for estimating the DC link voltage. The formulation of the observation problem as a parameter estimation problem and its solution by using the recursive least squares algorithm is presented in Section V. In Section VI, a fault diagnosis system for the DC link voltage sensor as well as a strategy for the reconfiguration of the control scheme are presented. In Section VII, experimental results are shown to demonstrate the effectiveness of the estimation methods, the fault diagnosis system and the reconfiguration strategy. Section VIII concludes this paper and shows possibilities regarding further research.

II. SYSTEM OVERVIEW

The considered system is a PMSM, that is controlled by a state of the art control loop in field oriented components. Fig. 1 shows a brief overview of the whole control loop. It consists of a cascade control for regulating the speed ω_m in the outer loop as well as the direct and quadrature axis currents (i_d and i_q) in the inner loop. The control signals are fed to a voltage source inverter (VSI) that applies the desired voltages to the PMSM. The pulse pattern for the VSI is generated by a sinusoidal pulse width modulation

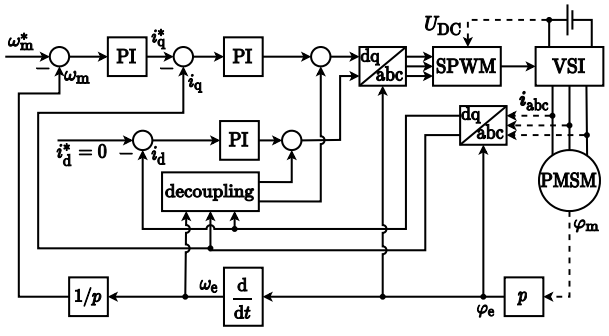

FIGURE 1. Overview of the control loop.

(SPWM). For the control algorithm to work properly, the three phase currents $\boldsymbol{i}_{\mathrm{abc}}$, the rotor position φ_{m} and the DC link voltage U_{DC} are measured (marked by dashed lines).

III. EFFECTS AND IMPACT OF AN INCORRECTLY MEASURED DC LINK VOLTAGE

In order to understand the impact of an incorrectly measured DC link voltage on the control performance, the q-axis current loop is considered as an example. The simplified q-axis control loop is shown in Fig. 2. In this representation the effects of switching, cross-coupling and park/clarke transformations are neglected for the sake of simplification.

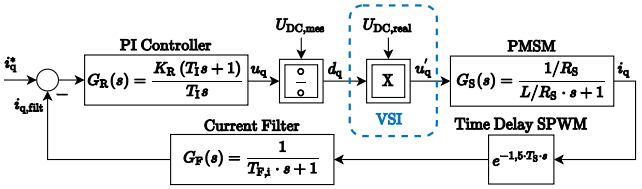

FIGURE 2. Simplified equivalent representation of the current control loop.

In Fig. 2, a PI controller with the transfer function

$$G_{\mathrm{R}}(s) = \frac{K_{\mathrm{R}}\,(T_{\mathrm{I}} \cdot s + 1)}{T_{\mathrm{I}} \cdot s} \tag{1}$$

generates a command voltage u_{q}. This voltage is divided by the measured DC link voltage $U_{\mathrm{DC,mes}}$ to receive the duty cycle d_{q}. The duty cycle is sent to the VSI, where it is used to apply the desired voltage to the PMSM. If the VSI is assumed to have ideal behavior, this process can be written by

$$u_{\mathrm{q}}^{'} = d_{\mathrm{q}} \cdot U_{\mathrm{DC,real}} \tag{2}$$

where $U_{\mathrm{DC,real}}$ is the real DC link voltage fed to the VSI. The PMSM as the plant is described by

$$G_{\mathrm{S}}(s) = \frac{\frac{1}{R_{\mathrm{S}}}}{\frac{L_{\mathrm{q}}}{R_{\mathrm{S}}} \cdot s + 1} = \frac{K_{\mathrm{A}}}{T_{\mathrm{A}} \cdot s + 1} \tag{3}$$

where R_{S} is the stator resistance and L_{q} is the quadrature axis inductance. Because of the sampling process and the voltage modulation by the SPWM method, there exists a time delay of $1.5 \cdot T_{\mathrm{S}}$ within the control loop, where T_{S} is the sample time. The measured phase currents in the stationary reference frame are transformed to rotor oriented coordinates in order to receive the currents i_{d} and i_{q}. The obtained current i_{q} is then filtered by a low pass with the transfer function:

$$G_{\mathrm{F}}(s) = \frac{1}{T_{\mathrm{F,i}} \cdot s + 1} \tag{4}$$

Generally, the Modulus Optimum (MO) based technique is used to design the current controller in frequency domain. $T_{\mathrm{I}} = \frac{L_{\mathrm{q}}}{R_{\mathrm{S}}}$ cancels the dominant pole of the plant with a controller zero. According to [18], a controller gain of

$$K_{\mathrm{R}} = \frac{T_{\mathrm{A}}}{2 \cdot K_{\mathrm{A}} \cdot T_{\sigma}} \tag{5}$$

where

$$T_{\sigma} = T_{\mathrm{F,i}} + 1.5 \cdot T_{\mathrm{S}} \tag{6}$$

maximizes the bandwidth of the control loop with a flat magnitude curve. This controller design is generally oscillation-free and robust with a nominal phase margin in the range of 65° to 70° (Fig. 3). The open-loop transfer function yields:

$$G_0(s) = G_{\mathrm{R}}(s) \cdot G_{\mathrm{S}}(s) \cdot \frac{U_{\mathrm{DC,real}}}{U_{\mathrm{DC,mes}}} \cdot e^{-1.5 \cdot T_{\mathrm{S}} \cdot s} \cdot G_{\mathrm{F}}(s) \tag{7}$$

In Fig. 3 the open-loop frequency response of $G_0(j\omega)$ with gains of $\frac{U_{\mathrm{DC,real}}}{U_{\mathrm{DC,mes}}} = 1$, $\frac{U_{\mathrm{DC,real}}}{U_{\mathrm{DC,mes}}} = 0.5$ and $\frac{U_{\mathrm{DC,real}}}{U_{\mathrm{DC,mes}}} = 5.2$ are compared. The latter case occurs when the DC link voltage gets measured too small by a factor of 5.2 (e.g. the real DC link voltage is 24 V, but the measurement provides a value of 4.62 V). The parameters of $G_0(s)$ are listed in Table 1.

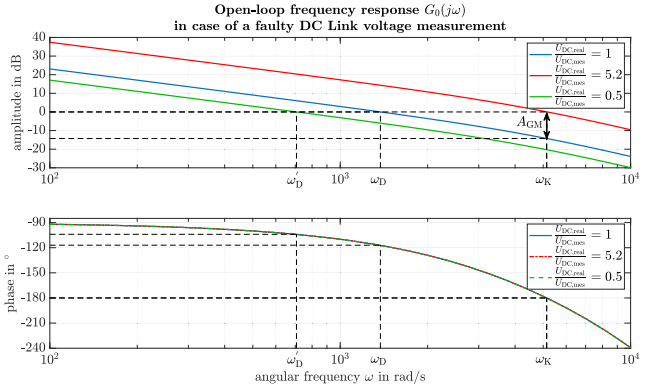

FIGURE 3. Open-loop frequency response $G_0(j\omega)$.

TABLE 1. Parameters of PMSM and Test Setup.

Parameter	Value
Stator Resistance R_{S}	0.25 Ω
Direct Axis Inductance L_{d}	0.1917 mH
Quadrature Axis Inductance L_{q}	0.2198 mH
Number of Pole Pairs p	4
Flux Linkage Ψ_{PM}	0.0119 Vs
Rated Torque T_{nom}	0.6 Nm
Inverter DC Link Voltage U_{DC}	24 V
Sample Time T_{S}	0.1 ms
Switching Frequency f_{SPWM}	10 kHz
Time Constant of Current Filter $T_{\mathrm{F,i}}$	0.2 ms
Proportional Gain of Current Controller K_{R}	0.3140
Integral Time Constant of Current Controller T_{I}	0.8792 ms

As it can be seen in Fig. 3, the open-loop frequency response with a correctly measured DC link voltage has a phase margin of 63° at a gain crossover frequency (GCF) of $\omega_{\mathrm{D}} = 1375$ rad/s. However, if the DC link voltage measurement is smaller than the real value by a factor of 5.2, the GCF increases to $\omega_{\mathrm{K}} = 5140$ rad/s. At this angular frequency, the phase of the open-loop frequency response is smaller than −180° leading to an unstable control loop. Therefore,

it can be concluded, that the control algorithm might become unstable, if the DC link voltage gets measured too small.

On the other hand, if the DC link voltage measurement is larger than the real value ($\frac{U_{\mathrm{DC,real}}}{U_{\mathrm{DC,mes}}} < 1$), the gain of the open loop decreases. This leads to a smaller GCF ($\omega_{\mathrm{D}}^{'} = 707$ rad/s) and a larger phase margin. Considering the stability of the control loop, it can be concluded that the control algorithm cannot become unstable, if the DC link voltage gets measured too large. However, a smaller gain crossover frequency causes a reduced speed of response. Consequently, a faulty DC link voltage measurement should always be reconfigured, so that the control algorithm operates with the actual DC link voltage. Thereby the stability of the control loop and its set dynamics are guaranteed at all times.

IV. ESTIMATION OF THE DC LINK VOLTAGE USING AN ADAPTIVE OBSERVER

A. BASIC PRINCIPLE OF A LUENBERGER OBSERVER

A Luenberger observer is used to estimate the state vector $\boldsymbol{x}$ of a linear system described by

$$\dot{\boldsymbol{x}} = \boldsymbol{A} \cdot \boldsymbol{x} + \boldsymbol{B} \cdot \boldsymbol{u} \tag{8}$$

$$\boldsymbol{y} = \boldsymbol{C} \cdot \boldsymbol{x} \tag{9}$$

where $\boldsymbol{u}$ is the input vector, $\boldsymbol{y}$ is the output vector and $\boldsymbol{A}$, $\boldsymbol{B}$, $\boldsymbol{C}$ are the system parameter matrices. According to [19], the state equations for the Luenberger observer are expressed as:

$$\dot{\hat{\boldsymbol{x}}} = \boldsymbol{A} \cdot \hat{\boldsymbol{x}} + \boldsymbol{B} \cdot \boldsymbol{u} + \boldsymbol{L} \cdot \left(\boldsymbol{y} - \hat{\boldsymbol{y}}\right) \tag{10}$$

$$\hat{\boldsymbol{y}} = \boldsymbol{C} \cdot \hat{\boldsymbol{x}} \tag{11}$$

Here $\hat{\boldsymbol{x}}$ and $\hat{\boldsymbol{y}}$ stand for the estimated values of the state and output vector, respectively. $\boldsymbol{L}$ as the observer gain has to be chosen during the design process. The observer error dynamics can be written by

$$\dot{\tilde{\boldsymbol{x}}} = (\boldsymbol{A} - \boldsymbol{L} \cdot \boldsymbol{C}) \cdot \tilde{\boldsymbol{x}} \tag{12}$$

where $\tilde{\boldsymbol{x}} = \boldsymbol{x} - \hat{\boldsymbol{x}}$. In order to ensure that the estimation error converges to zero, the observer poles have to be placed within the left half-plane using the observer gain matrix $\boldsymbol{L}$.

B. MODEL OF THE SYSTEM

Within this paper, the standard model of the PMSM in the rotating dq frame is used to describe its behavior:

$$u_{\mathrm{d}} = R_{\mathrm{S}} \cdot i_{\mathrm{d}} + L_{\mathrm{d}} \cdot \frac{\mathrm{d}i_{\mathrm{d}}}{\mathrm{d}t} - \omega_{\mathrm{e}} \cdot L_{\mathrm{q}} \cdot i_{\mathrm{q}} \tag{13}$$

$$u_{\mathrm{q}} = R_{\mathrm{S}} \cdot i_{\mathrm{q}} + L_{\mathrm{q}} \cdot \frac{\mathrm{d}i_{\mathrm{q}}}{\mathrm{d}t} + \omega_{\mathrm{e}} \cdot (L_{\mathrm{d}} \cdot i_{\mathrm{d}} + \Psi_{\mathrm{PM}}) \tag{14}$$

In equations (13) and (14), u_{d} and u_{q} refer to the command voltages of the current controllers, L_{d} and L_{q} are the direct and quadrature axis inductances, ω_{e} is the electrical angular velocity and Ψ_{PM} is the flux linkage. All other variables have already been explained.

Now equations (13) and (14) can be rearranged, so that both differential operators $\frac{\mathrm{d}i_{\mathrm{d}}}{\mathrm{d}t}$ and $\frac{\mathrm{d}i_{\mathrm{q}}}{\mathrm{d}t}$ are on the left side. Furthermore, the command voltages u_{d} and u_{q} will be replaced by

$$\begin{bmatrix} u_{\mathrm{d}} \\ u_{\mathrm{q}} \end{bmatrix} = \begin{bmatrix} d_{\mathrm{d}} \\ d_{\mathrm{q}} \end{bmatrix} \cdot U_{\mathrm{DC}} \tag{15}$$

where d_{d} and d_{q} are the duty cycles in the rotating dq frame. This yields:

$$\frac{\mathrm{d}i_{\mathrm{d}}}{\mathrm{d}t} = -\frac{R_{\mathrm{S}}}{L_{\mathrm{d}}} \cdot i_{\mathrm{d}} + \frac{L_{\mathrm{q}}}{L_{\mathrm{d}}} \cdot \omega_{\mathrm{e}} \cdot i_{\mathrm{q}} + \frac{1}{L_{\mathrm{d}}} \cdot d_{\mathrm{d}} \cdot U_{\mathrm{DC}} \tag{16}$$

$$\frac{\mathrm{d}i_{\mathrm{q}}}{\mathrm{d}t} = -\frac{R_{\mathrm{S}}}{L_{\mathrm{q}}} \cdot i_{\mathrm{q}} - \frac{L_{\mathrm{d}}}{L_{\mathrm{q}}} \cdot \omega_{\mathrm{e}} \cdot i_{\mathrm{d}} - \frac{\Psi_{\mathrm{PM}}}{L_{\mathrm{q}}} \cdot \omega_{\mathrm{e}} + \frac{1}{L_{\mathrm{q}}} \cdot d_{\mathrm{q}} \cdot U_{\mathrm{DC}} \tag{17}$$

Since U_{DC} as quantity to be estimated appears in both equations (16) and (17), it is sufficient to only consider the quadrature axis current i_{q} for the observer design. The DC link voltage U_{DC} can be seen as a disturbance that affects the system. Because U_{DC} is typically treated as a constant, its dynamics can be described by:

$$\frac{\mathrm{d}U_{\mathrm{DC}}}{\mathrm{d}t} = 0 \tag{18}$$

Equation (18) is a differential equation used to describe the dynamics of a constant disturbance affecting the system. Therefore, it is often called a disturbance model. Since the observer is designed to estimate this disturbance, the proposed observer is called disturbance observer in the following.

For the further procedure, the duty cycle d_{q} is interpreted as the system input u and the current i_{q} gets measured as the system output y. Besides, i_{q} and the DC link voltage U_{DC} are defined as elements of the state vector $\boldsymbol{x}$:

$$u = d_{\mathrm{q}}, \quad y = i_{\mathrm{q}}, \quad \boldsymbol{x} = \begin{bmatrix} i_{\mathrm{q}} \\ U_{\mathrm{DC}} \end{bmatrix} \tag{19}$$

By substituting equation (19) into the equations (17) and (18), the system dynamics can finally be written as:

$$\dot{\boldsymbol{x}} = \begin{bmatrix} \frac{d_{\mathrm{q}}}{L_{\mathrm{q}}} \cdot x_2 - \frac{R_{\mathrm{S}}}{L_{\mathrm{q}}} \cdot x_1 - \frac{L_{\mathrm{d}}}{L_{\mathrm{q}}} \cdot \omega_{\mathrm{e}} \cdot i_{\mathrm{d}} - \frac{\Psi_{\mathrm{PM}}}{L_{\mathrm{q}}} \cdot \omega_{\mathrm{e}} \\ 0 \end{bmatrix} \tag{20}$$

$$y = x_1 = \begin{bmatrix} 1 & 0 \end{bmatrix} \cdot \boldsymbol{x} = \boldsymbol{c}^{\mathrm{T}} \cdot \boldsymbol{x} \tag{21}$$

C. OBSERVABILITY AND OBSERVER DESIGN

Since the standard Luenberger observer is only defined for linear systems, but the state equation (20) of the system is nonlinear, the system dynamics are approximated by a linear parameter-varying (LPV) model with system matrix $\boldsymbol{A}$

$$\boldsymbol{A} = \frac{\mathrm{d}\dot{\boldsymbol{x}}}{\mathrm{d}\boldsymbol{x}} = \begin{bmatrix} -\frac{R_{\mathrm{S}}}{L_{\mathrm{q}}} & \frac{d_{\mathrm{q}}}{L_{\mathrm{q}}} \\ 0 & 0 \end{bmatrix} \tag{22}$$

where d_{q}, the duty cycle for the quadrature axis, is a time varying quantity.

In order to be able to design an observer, the considered LPV system has to be observable. This property of the system

can be checked by evaluating the observability matrix $\boldsymbol{Q}_\mathrm{B}$ as:

$$\boldsymbol{Q}_\mathrm{B} = \begin{bmatrix} \boldsymbol{c}^\mathrm{T} \\ \boldsymbol{c}^\mathrm{T} \cdot \boldsymbol{A} \end{bmatrix} = \begin{bmatrix} 1 & 0 \\ -\frac{R_\mathrm{S}}{L_\mathrm{q}} & \frac{d_\mathrm{q}}{L_\mathrm{q}} \end{bmatrix} \tag{23}$$

If the observability matrix $\boldsymbol{Q}_\mathrm{B}$ has full rank, the system is called observable and an observer can be designed [19]. Looking at equation (23), it can be seen that this is the case, if d_q is not zero. This condition is always fulfilled, because $|d_\mathrm{q}| > 0$ applies to all operating points except standstill with no load. Now an observer feedback vector $\boldsymbol{l}$ can be defined as

$$\boldsymbol{l} = \begin{bmatrix} l_1 \\ l_2/d_\mathrm{q} \end{bmatrix} \tag{24}$$

where l_1 and l_2 are parameters that can be chosen freely. The major advantage of this choice of vector $\boldsymbol{l}$ is that the eigenvalues of the observer are independent of d_q. Using the feedback, the observer error dynamics are set by $\boldsymbol{A}_\mathrm{GB}$:

$$\boldsymbol{A}_\mathrm{GB} = \boldsymbol{A} - \boldsymbol{l} \cdot \boldsymbol{c}^\mathrm{T} = \begin{bmatrix} -l_1 - \frac{R_\mathrm{S}}{L_\mathrm{q}} & \frac{d_\mathrm{q}}{L_\mathrm{q}} \\ -\frac{l_2}{d_\mathrm{q}} & 0 \end{bmatrix} \tag{25}$$

The eigenvalues λ_i (with $i = 1,\ 2$) of the matrix $\boldsymbol{A}_\mathrm{GB}$ are the zeros of its characteristic polynomial:

$$\det\left(\lambda \cdot \boldsymbol{I} - \boldsymbol{A}_\mathrm{GB}\right) = \lambda^2 + \lambda \cdot \frac{R_\mathrm{S} + L_\mathrm{q} \cdot l_1}{L_\mathrm{q}} + \frac{l_2}{L_\mathrm{q}} \tag{26}$$

The parameters l_1 and l_2 are calculated by comparing equation (26) with a desired polynomial that contains the desired eigenvalues. Within this paper, the eigenvalues are selected as:

$$\lambda_1 = -1136.4, \quad \lambda_2 = -2 \tag{27}$$

Hereby, λ_1 practically corresponds to the eigenvalue $-\frac{R_\mathrm{S}}{L_\mathrm{q}}$ of the considered LPV system from equation (22). The second eigenvalue of the system is zero. The eigenvalues of the LPV system can be calculated by solving the following equation:

$$\det\left(\lambda \cdot \boldsymbol{I} - \boldsymbol{A}\right) = 0 \tag{28}$$

For the estimation error to decrease faster than the system dynamics, the observer's second eigenvalue must be less than zero (in the left half-plane). At the same time however, the value must not lie too far in the left half-plane, otherwise the estimation signal of the observer might become very noisy. Therefore it was selected as $\lambda_2 = -2$. This leads to the following parameter values:

$$l_1 = 1, \quad l_2 = 0.5 \tag{29}$$

Using the observer feedback vector $\boldsymbol{l}$, the observer can be synthesized as

$$\dot{\hat{\boldsymbol{x}}} = \begin{bmatrix} \frac{d_\mathrm{q}}{L_\mathrm{q}}\hat{x}_2 - \frac{R_\mathrm{S}}{L_\mathrm{q}}\hat{x}_1 - \frac{L_\mathrm{d}}{L_\mathrm{q}}\omega_\mathrm{e} i_\mathrm{d} - \frac{\Psi_\mathrm{PM}}{L_\mathrm{q}}\omega_\mathrm{e} \\ 0 \end{bmatrix} + \begin{bmatrix} l_1 \\ \frac{l_2}{d_\mathrm{q}} \end{bmatrix} \cdot \left(i_\mathrm{q} - \hat{x}_1\right) \tag{30}$$

where i_d and i_q represent the measured direct and quadrature axis current and ω_e is the measured electrical angular velocity. The structure of the proposed observer is shown in Fig. 4.

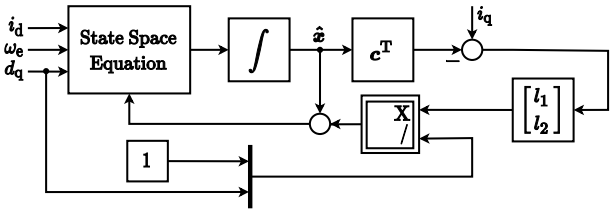

FIGURE 4. Proposed observer for estimating the DC link voltage.

Note: The adaptive feedback is necessary to ensure, that the eigenvalues of the observer are independent of d_q and its sign. It might be useful to implement a logic that effectively removes values of $d_\mathrm{q} = 0$ and replaces them with small values (e.g. $d_\mathrm{q} = 10^{-4}$) to avoid dividing by zero.

V. ESTIMATION OF THE DC LINK VOLTAGE USING A RECURSIVE LEAST SQUARES ALGORITHM

Apart from using an observer, the DC link voltage can also be estimated by a recursive least squares algorithm. Hereby, the DC link voltage is treated as an unknown parameter of an equation. By using the measurement information and input signal in the correct way, the parameter can be estimated.

A. BASIC PRINCIPLE OF LEAST SQUARES ALGORITHM

For designing the least squares (LS) algorithm, equation (17) gets rewritten in a different form:

$$L_\mathrm{q} \cdot \frac{\mathrm{d}i_\mathrm{q}}{\mathrm{d}t} + R_\mathrm{S} \cdot i_\mathrm{q} + L_\mathrm{d} \cdot \omega_\mathrm{e} \cdot i_\mathrm{d} + \Psi_\mathrm{PM} \cdot \omega_\mathrm{e} = d_\mathrm{q} \cdot U_\mathrm{DC} \tag{31}$$

Now the two parts independent of i_q on the left side of equation (31) are combined to a disturbance signal z.

$$L_\mathrm{q} \cdot \frac{\mathrm{d}i_\mathrm{q}}{\mathrm{d}t} + R_\mathrm{S} \cdot i_\mathrm{q} + z = d_\mathrm{q} \cdot U_\mathrm{DC} \tag{32}$$

Discretizing equation (32) using the forward Euler method and substituting U_DC with $\hat{U}_\mathrm{DC}$ yields:

$$\frac{L_\mathrm{q}}{T_\mathrm{S}}\left[i_\mathrm{q}(k) - i_\mathrm{q}(k-1)\right] + R_\mathrm{S} \cdot i_\mathrm{q}(k) + z(k) = \hat{U}_\mathrm{DC} \cdot d_\mathrm{q}(k) \tag{33}$$

Since the whole left side of equation (33) depends on the measured values of i_q, i_d and ω_e, this part is considered as the target value $x_\mathrm{T}(k)$. Besides, d_q is the system input $u(k)$, so that the model of the system can be written in the form of

$$x_\mathrm{T}(k) = \hat{U}_\mathrm{DC} \cdot u(k) \tag{34}$$

where $\hat{U}_\mathrm{DC}$ is the unknown DC link voltage which can be estimated using the LS algorithm. After a time interval of N sampling periods, the model can be shown in a vector form:

$$\begin{bmatrix} x_\mathrm{T}(1) \\ x_\mathrm{T}(2) \\ \vdots \\ x_\mathrm{T}(N) \end{bmatrix} = \begin{bmatrix} u(1) \\ u(2) \\ \vdots \\ u(N) \end{bmatrix} \cdot \hat{U}_\mathrm{DC} \quad \Rightarrow \quad \boldsymbol{x}_\mathrm{T} = \boldsymbol{u} \cdot \hat{U}_\mathrm{DC} \tag{35}$$

Now an LS algorithm can be used to choose $\hat{U}_{\mathrm{DC}}$ in a way, so that the sum of squared errors is minimized. According to [20] this leads to the following solution for $\hat{U}_{\mathrm{DC}}$:

$$\hat{U}_{\mathrm{DC}} = \left(\boldsymbol{u}^{\mathrm{T}} \cdot \boldsymbol{u}\right)^{-1} \cdot \boldsymbol{u}^{\mathrm{T}} \cdot \boldsymbol{x}_{\mathrm{T}} \tag{36}$$

B. EXTENSION TO RECURSIVE LEAST SQUARES ALGORITHM

In certain scenarios it is useful to arrange the LS algorithm recursively. This keeps the computational burden at a constant level although new samples for the input and output signals are fed to the algorithm. Therefore, this extension is called recursive least squares (RLS) algorithm. The basic idea of RLS is to let the current estimate for the unknown parameter $\hat{U}_{\mathrm{DC}}$ at sample point k depend on all the data achieved previously, without adding further values to the vectors $\boldsymbol{u}$ and $\boldsymbol{x}_{\mathrm{T}}$. The RLS algorithm describes how the estimated unknown parameter $\hat{U}_{\mathrm{DC}}(k-1)$ at sample point $k-1$ is updated to $\hat{U}_{\mathrm{DC}}(k)$, once the new values for $u(k)$ and $x_{\mathrm{T}}(k)$ are obtained. According to [20] and [21] this procedure can be described by:

$$\hat{U}_{\mathrm{DC}}(k) = \hat{U}_{\mathrm{DC}}(k-1) + \boldsymbol{K}(k) \cdot e(k) \tag{37}$$

$$e(k) = x_{\mathrm{T}}(k) - u(k) \cdot \hat{U}_{\mathrm{DC}}(k-1) \tag{38}$$

$$\boldsymbol{K}(k) = \frac{\boldsymbol{P}(k-1) \cdot u(k)}{\lambda + u^2(k) \cdot \boldsymbol{P}(k-1)} \tag{39}$$

$$\boldsymbol{P}(k) = \frac{1}{\lambda}\left[\boldsymbol{P}(k-1) - \frac{\boldsymbol{P}^2(k-1) \cdot u^2(k)}{\lambda + u^2(k) \cdot \boldsymbol{P}(k-1)}\right] \tag{40}$$

Hereby $\boldsymbol{K}(k)$ denotes the gain matrix, $\boldsymbol{P}(k)$ is the covariance matrix and $0 < \lambda < 1$ stands for the adjustable forgetting factor. The structure of the RLS algorithm is shown in Fig. 5. Within this paper, the default values are set to $\hat{U}_{\mathrm{DC}}(0) = 0$ and $\boldsymbol{P}(0) = 10^4$. The forgetting factor is chosen as $\lambda = 0.97$.

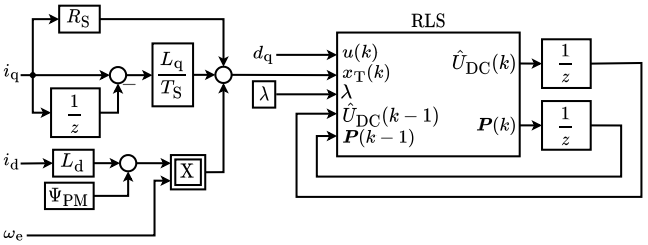

FIGURE 5. RLS algorithm for estimating the DC link voltage.

Note: Although $\boldsymbol{K}(k)$ and $\boldsymbol{P}(k)$ are scalar variables within this paper, they typically represent matrices. For the sake of simplicity, they are nevertheless marked with bold capital letters to prevent misunderstanding. Furthermore, it must be considered that the equations (37) - (40) have already been simplified because $e(k)$, $u(k)$, $x_{\mathrm{T}}(k)$, $\boldsymbol{K}(k)$ and $\boldsymbol{P}(k)$ are scalar quantities.

VI. FAULT DIAGNOSIS OF DC LINK VOLTAGE AND RECONFIGURATION

A. FAULT CATEGORIES AND THEIR CAUSE

The diagnosis system developed in the following is capable of detecting two different fault categories. The fault scenarios can be derived based on the measurement method using a differential amplifier as shown in Fig. 6.

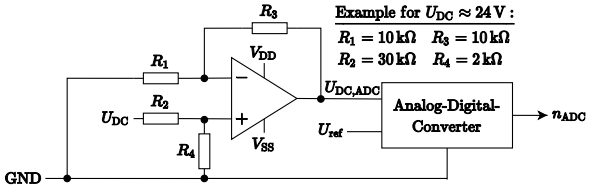

FIGURE 6. Differential amplifier for measuring the DC link voltage.

The gain k_{ADC} between the actual DC link voltage U_{DC} and the voltage $U_{\mathrm{DC,ADC}}$ fed to the Analog-Digital-Converter (ADC) yields:

$$k_{\mathrm{ADC}} = \frac{U_{\mathrm{DC,ADC}}}{U_{\mathrm{DC}}} = \frac{R_4}{R_2 + R_4} \cdot \frac{R_1 + R_3}{R_1} = 0.125 \tag{41}$$

The ADC compares the voltage $U_{\mathrm{DC,ADC}}$ to a reference voltage (e.g. $U_{\mathrm{ref}} = 3.3$ V) and generates a number n_{ADC} between 0 and $2^{Bits_{\mathrm{ADC}}} - 1$ where $Bits_{\mathrm{ADC}}$ refers to the number of bits used for the analog-digital-conversion. The measured DC link voltage $U_{\mathrm{DC,mes}}$ can then be calculated as:

$$U_{\mathrm{DC,mes}} = \frac{n_{\mathrm{ADC}}}{2^{Bits_{\mathrm{ADC}}} - 1} \cdot U_{\mathrm{ref}} \cdot \frac{1}{k_{\mathrm{ADC}}} \tag{42}$$

As it can be seen in Fig. 6, the voltage $U_{\mathrm{DC,ADC}}$ fed to the ADC will tend to zero, if the resistor R_2 breaks and becomes high impedant. The same effect can occur because of solder fatigue at the solder joints of R_2. Since $U_{\mathrm{DC,ADC}}$ tends to zero, also the value for the measured DC link voltage $U_{\mathrm{DC,mes}}$ eventually reaches zero. Therefore, this fault is considered as a complete sensor failure with the following failure model:

$$U_{\mathrm{DC,ADC}} = U_{\mathrm{DC,mes}} = 0 \ll U_{\mathrm{DC,real}} \tag{43}$$

Similar to what was described before, one of the other resistors in Fig. 6 can also fail and become high impedant. As an example, it is assumed that R_1 fails and after the fault occurs, the value equals $R_1^{'} = 1$ MΩ. This changes the amplification factor to:

$$k_{\mathrm{ADC}}^{'} = \frac{U_{\mathrm{DC,ADC}}}{U_{\mathrm{DC}}} = \frac{R_4}{R_2 + R_4} \cdot \frac{R_1^{'} + R_3}{R_1^{'}} \approx 0.063 \tag{44}$$

Compared with the gain factor 0.125 from equation (41), the voltage $U_{\mathrm{DC,ADC}}$ is now only about half of the value before the fault occurred, if the actual DC link voltage U_{DC} remains unchanged. Consequently, the measured DC link voltage $U_{\mathrm{DC,mes}}$ also decreases to half of its value, since k_{ADC} is still used in the software to calculate the DC link voltage based on the ADC information. This fault scenario can

be interpreted as a gain fault. Mathematically, this can be expressed as:

$$0 \ll U_{\mathrm{DC,mes}} \neq U_{\mathrm{DC,real}} \tag{45}$$

There are a lot of other fault scenarios to be thought of. Still, they all have the same effect of an incorrectly measured DC link voltage. Since U_{DC} is typically considered to be constant, a distinction between offset and gain faults is not useful. Because of that, all significant deviations of the measured DC link voltage $U_{\mathrm{DC,mes}}$ from the actual value U_{DC} (with $U_{\mathrm{DC,mes}} > 0$) are considered as a sensor deviation, which is the second fault scenario.

B. FAULT DIAGNOSIS SYSTEM

The proposed fault diagnosis systems uses two flags to indicate the fault category. A complete sensor failure is detected if the measured DC link voltage $U_{\mathrm{DC,mes}}$ is smaller than a set threshold $th_{\mathrm{fail-DC}}$. The second fault is assumed to be a deviation between measured and estimated DC link voltage, with the measured value still being above the previously mentioned threshold.

Considering the analysis in section III, a faulty measurement (especially a complete sensor failure) has to be detected before the system becomes unstable. Therefore, $th_{\mathrm{fail-DC}}$ should not be chosen too small, but rather dependent on the nominal DC link voltage $U_{\mathrm{DC,nom}}$ and the open-loop frequency response. As Fig. 3 shows, the gain margin of the open-loop frequency response with the DC link voltage measured correctly is approximately $A_{\mathrm{GM}} \approx 14.25$ dB at a phase crossover frequency $\omega_{\mathrm{K}} = 5140$ rad/s. Based on this value, it is clear, that the control loop becomes unstable if the DC link voltage gets measured too small by a factor of

$$k_{\mathrm{crit}} = \frac{1}{10^{-A_{\mathrm{GM}}/20}} = \frac{1}{10^{-14.25/20}} \approx 5.16 \tag{46}$$

This is the case, when the measurement value drops below the threshold

$$th_{\mathrm{fail-DC}} = \frac{U_{\mathrm{DC,nom}}}{k_{\mathrm{crit}}} = \frac{24\,\mathrm{V}}{5.16} = 4.65\,\mathrm{V} \tag{47}$$

while the actual DC link voltage remains at its nominal value. To detect this sensor fault before the control loop becomes unstable, some kind of trade-off is necessary. On the one hand, the parameter should be chosen relatively high to allow for a fast detection, preventing an unstable operation. On the other hand, a value close to the threshold given in equation (47) minimizes the number of false alarms. To be on the safe side and allow for a faster fault detection time, the parameter will be selected as:

$$th_{\mathrm{fail-DC}} = 10\,\mathrm{V} \tag{48}$$

If the previously mentioned condition

$$U_{\mathrm{DC,mes}} < th_{\mathrm{fail-DC}} \tag{49}$$

is fulfilled, a flag $Flag_{\mathrm{fail-DC}}$ is set to signalize the presence of the fault.

The other fault scenario, a deviation between measured and estimated DC link voltage, is detected if the following conditions are true:

- The flag $Flag_{\mathrm{fail-DC}}$ is not set. Therefore, the voltage sensor is assumed to not have failed completely.
- The absolute difference between the measured DC link voltage $U_{\mathrm{DC,mes}}$ and its estimated value $\hat{U}_{\mathrm{DC}}$ exceeds a set threshold $th_{\mathrm{dev-DC}}$ for a minimum time span of $t_{\mathrm{min,dev-DC}}$. Both parameters affect the sensitivity of the diagnosis system and the required time to detect a faulty measurement. Ideally, the parameters should be chosen quite small allowing a fast detection of even very small faults. However, small values also increase the risk of false alarms during transients of speed, current and load. By using suitable values for $th_{\mathrm{dev-DC}}$ and $t_{\mathrm{min,dev-DC}}$ these transients, which can lead to deviations between $U_{\mathrm{DC,mes}}$ and $\hat{U}_{\mathrm{DC}}$ even in the non-fault case, are being ignored. In this paper, a compromise is made and the parameters are selected as:

$$th_{\mathrm{dev-DC}} = 1\,\mathrm{V}, \quad t_{\mathrm{min,dev-DC}} = 50\,\mathrm{ms} \tag{50}$$

If both conditions are fulfilled, a flag $Flag_{\mathrm{dev-DC}}$ is set to indicate the fault. The proposed diagnosis system for the DC link voltage is shown in Fig. 7.

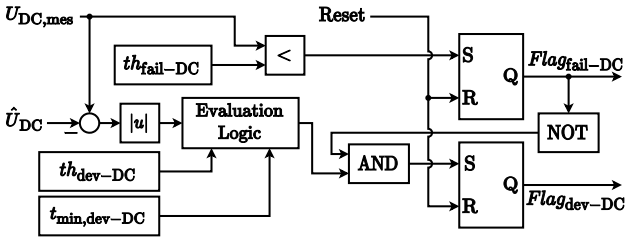

FIGURE 7. Structure of the fault diagnosis system.

Note: A complete sensor failure is assumed to occur rapidly, so that the measured DC link voltage $U_{\mathrm{DC,mes}}$ decreases to a value lower than $th_{\mathrm{fail-DC}}$ in a shorter time than $t_{\mathrm{min,dev-DC}}$. As long as the software-based time constant for filtering the measured DC link voltage is not chosen too big, this assumption should always be met. This way the flag $Flag_{\mathrm{fail-DC}}$ is always set before the second condition for enabling the flag $Flag_{\mathrm{dev-DC}}$ is true. This makes it possible to distinguish between the two fault scenarios.

C. RECONFIGURATION OF FAULTY DC LINK VOLTAGE MEASUREMENT

As shown in Section III, a faulty DC link voltage measurement deteriorates control performance or even leads to instability of the control system. Therefore, in this case the measured DC link voltage $U_{\mathrm{DC,mes}}$ used for calculating the duty cycle by the SPWM method should always be replaced with the estimated value $\hat{U}_{\mathrm{DC}}$. Two flags ($Flag_{\mathrm{fail-DC}}$ and $Flag_{\mathrm{dev-DC}}$) have been introduced for indicating the considered fault scenarios. Hence, the reconfiguration strategy

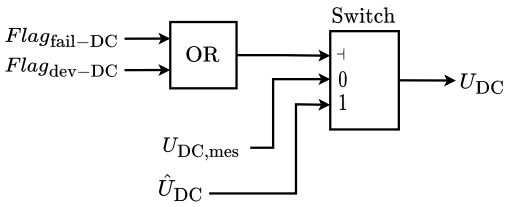

FIGURE 8. Reconfiguration of a faulty DC link voltage measurement.

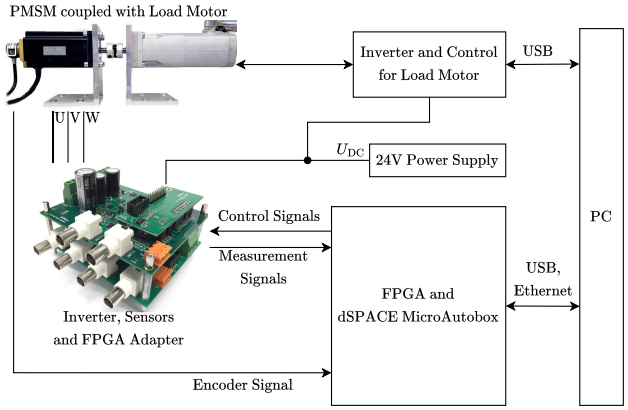

FIGURE 9. Structure of the experimental hardware setup.

is quite simple. If at least one of the flags is set, the DC link voltage used for the control algorithm is switched from $U_{\text{DC,mes}}$ to $\hat{U}_{\text{DC}}$. The implemented logic is shown in Fig. 8.

VII. EXPERIMENTAL RESULTS

To assess the performance of the proposed estimation schemes, the fault diagnosis system and the reconfiguration strategy, various experiments are performed on a hardware setup shown in Fig. 9. Therefore, these four software modules as well as the control algorithm are implemented on a real-time system consisting of an FPGA and a dSPACE MicroAutoBox. The experiments are performed by using a 24 V inverter and a small PMSM coupled with a load motor. Details regarding the used PMSM have already been shown in Table 1.

At first, the observer and the RLS algorithm for estimating the DC link voltage are compared. Then, two measurement results are presented to show the effectiveness of the fault diagnosis system and the reconfiguration strategy. All three measurements have been performed at 50% of the rated torque.

A. COMPARISON OF OBSERVER AND RLS ALGORITHM

Since two methods (disturbance observer from section IV and RLS algorithm from section V) have been proposed for estimating the DC link voltage, it is useful to compare their performance. Their dynamic and steady state behavior is considered in Fig. 10. Since the DC link voltage is typically seen as a constant, the best approach to compare the two estimation schemes regarding their dynamic behavior is to

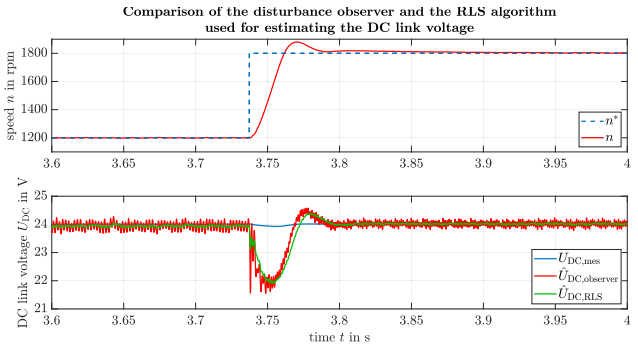

FIGURE 10. Comparison of disturbance observer and RLS algorithm.

investigate the estimated signals after a reference step of the motor speed.

As Fig. 10 shows, both approaches share pretty much the same dynamics after a change of the motor speed. Following the speed reference step from 1200 rpm to 1800 rpm at time $t = 3.74$ s, the estimation converges to the correct value within approximately 60 ms. So both methods have nearly the same dynamic behavior. However it can be noticed, that the disturbance observer has a much more recognizable tendency to oscillations than the RLS method. This is an advantage of the latter approach, since no filtering of the estimated signal $\hat{U}_{\text{DC,RLS}}$ is required. To smooth the signal $\hat{U}_{\text{DC,observer}}$, a low pass filter can be used. Alternatively, the magnitude of the observer eigenvalues can be reduced. This leads to less oscillations, but also reduces the estimation error dynamics.

As the DC link voltage is typically seen as a constant, it is nevertheless useful to implement a low pass filter with a time constant of 5 ms for both approaches. This way, both methods provide even more similar results and a smooth estimated signal for the DC link voltage. Still, one drawback of the method currently is the deviation between measured and estimated DC link voltage in case of dynamic changes regarding the operating point. This behavior has to be investigated in future research.

B. DIAGNOSIS AND RECONFIGURATION EXPERIMENTAL RESULTS

Now two experimental results are presented to demonstrate the function of the diagnosis system and the reconfiguration method. Hereby, a fault is injected by manipulating the correct information of the ADC yielding a faulty measurement value. Fig. 11 shows a measurement result where the DC link voltage sensor fails completely. Then the presented reconfiguration strategy is used to replace the faulty measurement with the estimated value of the disturbance observer. However, the obtained value of the observer fed to the fault diagnosis system and reconfiguration strategy can easily be replaced by the estimated value of the RLS algorithm as well. Since both estimated values for $\hat{U}_{\text{DC}}$ of the observer and the RLS algorithm are filtered by a low pass with a time constant

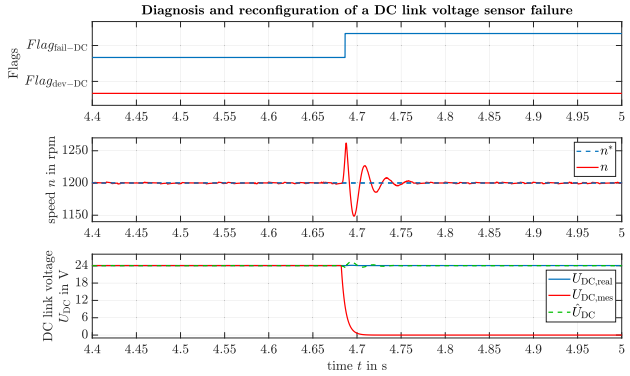

FIGURE 11. Reconfiguration of a DC link voltage sensor failure.

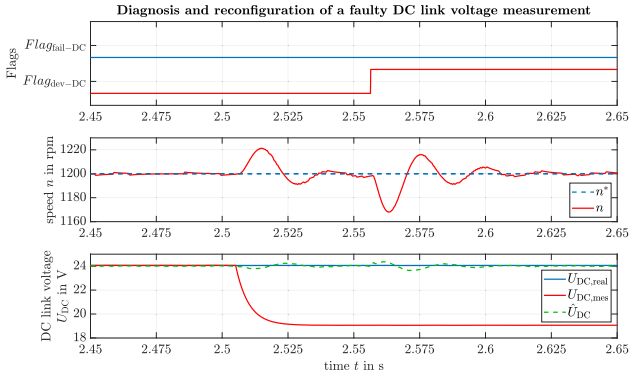

FIGURE 12. Reconfiguration of a faulty DC link voltage measurement.

of 5 ms, their dynamic and steady state behavior is very similar.

At the beginning, the motor speed equals $n = 1200$ rpm where the measured DC link voltage $U_{\text{DC,mes}}$ is used for the control algorithm as shown in Fig. 2. Both, the measured and the estimated values of the DC link voltage $\hat{U}_{\text{DC}}$ are in good agreement with the actual value $U_{\text{DC,real}}$. However, at $t = 4.675$ s the DC link voltage sensor fails and the measured value $U_{\text{DC,mes}}$ decreases to zero within roughly 25 ms as the time constant for filtering the DC link voltage is set to $T_{\text{F,DC}} = 5$ ms. Because the threshold for detecting a failure of the DC link voltage sensor was set to $th_{\text{fail-DC}} = 10$ V, the fault is detected as soon as $U_{\text{DC,mes}}$ falls below 10 V. The diagnosis system enables the flag $Flag_{\text{fail-DC}}$ and the reconfiguration strategy replaces $U_{\text{DC,mes}}$ with $\hat{U}_{\text{DC}}$ for the control algorithm. As it can be seen in the second plot, there is a small oscillation in the speed signal which disappears approximately 10 ms after the fault occurred. The oscillation is mainly evoked due to the harsh and simple switching from $U_{\text{DC,mes}}$ to $\hat{U}_{\text{DC}}$. Further studies regarding more advanced reconfiguration strategies are needed. Because of the reconfiguration algorithm and $\hat{U}_{\text{DC}} \approx U_{\text{DC,real}}$, the motor can continue to operate safely with the same control dynamics despite the sensor failure.

The second measurement result in Fig. 12 shows the diagnosis and reconfiguration of a faulty DC link voltage measurement. This time however, the sensor does not fail completely, but rather suffers a wrong gain factor as discussed in section VI. This leads to an incorrectly measured value for the DC link voltage with $0 \ll U_{\text{DC,mes}} < U_{\text{DC,real}}$. Due to the incorrect amplification factor, the measured value for the DC link voltage $U_{\text{DC,mes}}$ drops from 24 V to 19 V at $t \approx 2.5$ s. Because the estimated value for the DC link voltage remains at 24 V after the fault, the difference between the measured and the estimated values exceeds the set threshold of $th_{\text{dev-DC}} = 1$ V as stated in equation (50). Since the difference continues to have a value greater than $th_{\text{dev-DC}}$ for a time span longer than $t_{\text{min,dev-DC}} = 50$ ms, the fault is detected at $t \approx 2.55$ s. The diagnosis system enables the flag $Flag_{\text{dev-DC}}$ and the reconfiguration algorithm replaces $U_{\text{DC,mes}}$ with $\hat{U}_{\text{DC}}$, which is estimated by the observer.

As the second plot shows, the oscillation in the measured speed signal n is triggered by two events. The first event at $t = 2.51$ s is caused by the fault occurrence, when due to the sensor fault, the measured value $U_{\text{DC,mes}}$ drops to 19 V. During the time span $2.51\,\text{s} \leq t \leq 2.56\,\text{s}$, the faulty measurement is still used to control the motor as shown in Fig. 2. However, due to the fact that the factor

$$k = \frac{U_{\text{DC,real}}}{U_{\text{DC,mes}}} = \frac{24\,\text{V}}{19\,\text{V}} \approx 1.26 < 5.16 = k_{\text{crit}} \tag{51}$$

is smaller than its critical value k_{crit}, the control loop remains stable. As a consequence, the oscillation is damped and the motor speed becomes steady at its reference value. In the meantime, the fault is detected and isolated by the diagnosis system. The reconfiguration scheme in the control algorithm switches the value of the DC link voltage from the faulty value of 19 V to the estimated value of 24 V (at $t = 2.56$ s). This sudden change causes another damped oscillation. Of course, this reconfiguration strategy which causes a switching in the system is not optimal. In the future, the reconfiguration could be improved to implement a soft transition from $U_{\text{DC,mes}}$ to $\hat{U}_{\text{DC}}$.

Note: The reconfiguration of the sensor failure in Fig. 11 is mandatory, because otherwise the control loop would become unstable. The reconfiguration of the second fault scenario in Fig. 12 however is optional, if only instability concerns are considered. As it can be seen in the second plot of Fig. 12, the control loop is able to reach its reference value after the fault occurred, even if the faulty measured value $U_{\text{DC,mes}}$ is used for controlling the motor. Stability of the control loop is no problem in this case. Nevertheless, the reconfiguration of the faulty DC link voltage measurement is still useful in order to keep the closed loop dynamics set by the controller design.

VIII. CONCLUSION

Controlled PMSM drives rely on the measurements of current, speed and DC link voltage. In practice, the sensors used for acquiring these measurements can provide false values or fail completely, with a significant impact on the control behavior. This paper discussed the impact of an incorrectly measured DC link voltage on a synchronous drive system,

controlled by a cascade control in field oriented coordinates. The analysis showed that the control algorithm can become unstable if the DC link voltage gets measured too small, because the gain of the open loop increases. This leads to a smaller phase margin, eventually resulting in an unstable control loop. Therefore, two methods were proposed to estimate the DC link voltage based on the measured currents, the rotor speed and the duty cycle. Furthermore, a fault diagnosis system was introduced, capable of detecting a faulty DC link voltage sensor. A reconfiguration algorithm replaces the faulty measurement with the estimated value. Experimental results show the effectiveness of the two estimation algorithms, the fault diagnosis system and the reconfiguration strategy.

When comparing the results to others works, the proposed observers not only have the advantage of providing an estimated value for the measured quantity instead of purely supervising the measurement by a power balance equation. Additionally, the observers only rely on measurement signals, that are needed for control anyway and do not require any further sensors to be added to the system. Lastly, the fault detection and reconfiguration method can be tuned by three simple and physically interpretable parameters.

In this paper the algorithms were developed assuming the nominal system. In practice, there may be the influence of certain factors such as interference noise which will impact the system. Therefore, future research has to be done regarding the influence of disturbances on the estimation accuracy and the fault detection robustness. Additionally, the error of both estimation schemes at changing operating conditions of the drive system has to be examined in more detail.

REFERENCES

[1] Y. Chen, S. Liang, W. Li, H. Liang, and C. Wang, "Faults and diagnosis methods of permanent magnet synchronous motors: A review," *Appl. Sci.*, vol. 9, no. 10, p. 2116, May 2019.
[2] F. Grouz, L. Sbita, and M. Boussak, "Current sensors faults detection, isolation and control reconfiguration for PMSM drives," in *Proc. Int. Conf. Electr. Eng. Softw. Appl.*, 2013, pp. 1–6.
[3] M. H. Salem, Y. Bensalem, and M. N. Abdelkrim, "A speed sensor fault tolerant control for a permanent magnet synchronous motor," in *Proc. 17th Int. Multi-Conf. Syst., Signals Devices (SSD)*, 2020, pp. 290–295.
[4] G. Huang, J. She, E. F. Fukushima, C. Zhang, and J. He, "Robust reconstruction of current sensor faults for PMSM drives in the presence of disturbances," *IEEE/ASME Trans. Mechatronics*, vol. 24, no. 6, pp. 2919–2930, Dec. 2019.
[5] M. Laumann, C. Weiner, and R. Kennel, "Current sensorless field oriented control of a RSM by extended-Kalman-filter based state estimation," in *Proc. IEEE 10th Int. Symp. Sensorless Control Electr. Drives (SLED)*, Sep. 2019, pp. 1–6.
[6] A. Abderrezak and K. Madjid, "Sensor fault detection, localization, and system reconfiguration with a sliding mode observer and adaptive threshold of PMSM," *J. Power Electron.*, vol. 16, no. 3, pp. 1012–1024, May 2016.
[7] S. X. Ding, *Model-Based Fault Diagnosis Techniques*. Berlin, Germany: Springer, 2008.
[8] P. M. Frank, "Fault diagnosis in dynamic systems using analytical and knowledge-based redundancy: A survey and some new results," *Automatica*, vol. 26, no. 3, pp. 459–474, May 1990.
[9] J. J. Gertler, "Survey of model-based failure detection and isolation in complex plants," *IEEE Control Syst. Mag.*, vol. 8, no. 6, pp. 3–11, Dec. 1988.
[10] M. Blanke, M. Kinnaert, J. Lunze, and M. Staroswiecki, *Diagnosis and Fault-Tolerant Control*, 3rd ed. Berlin, Germany: Springer, 2016.
[11] I. Hwang, S. Kim, Y. Kim, and C. E. Seah, "A survey of fault detection, isolation, and reconfiguration methods," *IEEE Trans. Control Syst. Technol.*, vol. 18, no. 3, pp. 636–653, May 2010.
[12] R. Isermann and P. Ballé, "Trends in the application of model-based fault detection and diagnosis of technical processes," *Control Eng. Pract.*, vol. 5, no. 5, pp. 709–719, 1997.
[13] Y.-S. Jeong, S.-K. Sul, S. Schulz, and N. Patel, "Fault detection and fault tolerant control of interior permanent magnet motor drive system for electric vehicle," in *Proc. 38th IAS Annu. Meeting Conf.*, 2003, pp. 1458–1463.
[14] S. Diao, D. Diallo, and E. Laboure, "A nonlinear observer for DC bus voltage estimation and sensor diagnosis for a battery charger used in automotive systems," in *Proc. IEEE 24th Int. Symp. Ind. Electron. (ISIE)*, Jun. 2015, pp. 438–443.
[15] S. Diao, "Fault tolerant control for critical machine-inverter systems used in automotive industry," Ph.D. dissertation, Dept. Eng. Sci., Université Paris, Paris, France, 2014. Accessed: Jun. 30, 2021.
[16] G. H. B. Foo, X. Zhang, and D. M. Vilathgamuwa, "A sensor fault detection and isolation method in interior permanent-magnet synchronous motor drives based on an extended Kalman filter," *IEEE Trans. Ind. Electron.*, vol. 60, no. 8, pp. 3485–3495, Aug. 2013.
[17] S.-C. Kim, T. H. Nguyen, D.-C. Lee, K.-B. Lee, and J.-M. Kim, "Fault tolerant control of DC-link voltage sensor for three-phase AC/DC/AC PWM converters," *J. Power Electron.*, vol. 14, no. 4, pp. 695–703, Jul. 2014.
[18] D. Schröder, *Elektrische Antriebe—Regelung von Antriebssystemen*, 4th ed. Berlin, Germany: Springer, 2015.
[19] D. Luenberger, "An introduction to observers," *IEEE Trans. Autom. Control*, vol. AC-16, no. 6, pp. 596–602, Dec. 1971.
[20] R. Krneta, S. Antic, and D. Stojanovic, "Recursive least squares method in parameters identification of DC motors models," *Facta Universitatis, Electron. Energetics*, vol. 18, no. 3, pp. 467–478, 2005.
[21] L. Ljung, *System Identification: Theory for the User*, 2nd ed. Upper Saddle River, NJ, USA: Prentice-Hall, 1999.

PHILIPP HEIL was born in Fulda, Germany, in 1996. He received the B.Eng. and M.Eng. degrees in electrical engineering from the Technical University of Applied Sciences Würzburg-Schweinfurt, Germany, in 2020 and 2021, respectively.

After completing the B.Eng. degree, he was a Student Assistant with the Laboratory for Control Systems, Department of Electrical Engineering, Technical University of Applied Sciences Würzburg-Schweinfurt. He is currently a development engineer in the automotive industry. His research interests include the observer structures for estimating the state of controlled electrical drives and the fault diagnosis of sensor faults in electric drive systems.

ABID ALI received the B.Sc. degree in electrical engineering from the University of Engineering and Technology Lahore, Pakistan, in 1991, and the master's and Ph.D. degrees from Ruhr-Universität Bochum, Germany, in 1998 and 2003, respectively.

After completing the B.Sc. degree, he was with the power engineering industry for a few years. In 2003, he joined the automotive industry. Currently, he is a Professor in control systems with the Department of Electrical Engineering, Technical University of Applied Sciences Würzburg-Schweinfurt. His current research interests include the self-sensing and fault-tolerant control of electrical drives, adaptive and learning techniques, and automotive controls.